COBEM 2023 27TH INTERNATIONAL CONGRESS OF MECHANICAL ENGENEERING

ABCM Brazilian Society of Mechanical Sciences and Engineering
27th ABCM International Congress of Mechanical Engineering
December 04-08, 2023, Florianópolis-SC, Brazil

COB-2023-1508
DESIGN AND PERFORMANCE ANALYSIS OF A FRANCIS TYPE HYDRAULIC TURBINE IMPELLER USING CFD

Mateus Felipe Benicio Moraes[1]
Dener Silva de Almeida[2]
[1]Instituto Federal do Maranhão, Av. Getúlio Vargas, 04 - Monte Castelo, São Luís - MA, 65030-005
[2]Universidade Federal do Maranhão, Av. dos Portugueses, 1966 - Vila Bacanga, São Luís - MA, 65080-805

mateusmoraes@acad.ifma.edu.br
dener.almeida@ufma.br

Abstract. *The impeller is the component of the hydraulic turbine responsible for converting hydraulic energy into mechanical energy. It consists of a series of specially shaped blades that use the movement of water to create a torque that enables it to rotate. The device's geometry is determined through the design process, but this procedure does not provide a satisfactory understanding of the flow properties such as velocity and pressure. Computation Fluid Dynamics (CFD) is a versatile and cost-effective tool for experimental tests that can analyse various impellers in different operating conditions. This work aimed at designing the impeller of a Francis turbine using the Bovet method and analysing flow (pressure and velocity) and performance (head, power, efficiency, torque, and characteristic curves) parameters through a simulation in the software Ansys Student 2023 R2. Turbomachinery Fluid Flow and its modules BladeGen, TurboMesh, CFX-Pre and CFX-Post were used to simulate fluid flow and obtain the impeller's performance parameters. The simulations were carried out in nine meshes to investigate mesh convergence. A k-ε model and the high resolution advection scheme were used to calculate the fluid flow. The results showed that fluid particles collided with the blades and were projected in the rotation direction. Mesh convergence couldn't be verified. Flow separation and vortex formation between the blades occurred. There was a low-pressure zone at the blade's leading edge, a behaviour that tends to induce cavitation and damage Francis turbine impellers in this region. The head value was overestimated due to numerical instabilities. The efficiency was lower due to impact losses, flow separation, and vortices. Shaft power and torque presented close errors due to error propagation. The efficiency curve showed only increasing trends, not behaving as expected. The relative errors of the performance parameters were about 11%.*

Keywords: *francis turbine, design, simulation, performance.*

1. INTRODUCTION

Hydraulic energy is found in rivers, seas, and streams as potential or kinetic energy (Henn, 2006). In 2021, it was employed to generate 15.01 % of all electricity worldwide, being the most used renewable energy source. The three countries that most use this energy source are China, Canada, and Brazil, accounting for 30.42%, 8.91%, and 8.49% of all electricity generated by this means in 2021, respectively (British Petroleum Company, 2022). This source is usually carried out in hydroelectric plants, facilities where water is stored and transported to hydraulic turbines, and devices that convert hydraulic energy into mechanical energy, which is later converted into electrical energy.

In Brazil, 1372 hydroelectric power plants are in operation, of which 216 are Hydroelectric Power Plants, 424 are Small Hydroelectric Power Plants, and 732 are Hydroelectric Generating Plants (ANEEL, 2022). In 2021, this set of power plants was responsible for 11% of the energy matrix and 56.8% of the electrical matrix (EPE, 2022).

The impeller is the component of the turbine that converts hydraulic energy into mechanical energy, so it must be correctly designed to ensure its proper use. The design process is a series of calculations where the impeller's geometric and operational parameters are determined, providing the necessary data for its design and manufacture. However, during this process, parameters related to the impeller's performance, such as flow velocity, streamlines, and pressure distribution along the blades, are not fully known. These parameters can be obtained by simulations carried out by commercial software, making it possible to adjust the geometry to achieve the desired performance.

Previous works prove the accuracy of computational analysis, such as the one developed by Wu *et al.* (2007), which employed a CFD-based design system combining three blade design methods, a parameterised geometry model, an automatic mesh generator, and CFD software to rehabilitate a Francis turbine. The inviscid Q3D codes were used in the preliminary optimisation due to their high convergence rate and reliability. The commercial simulation software STAR-CD was used in the final phase. The design improvements provided a 23% increase in generated power, a 3% increase in maximum efficiency, a lower cavitation coefficient, and smoother performance over a wide range of operating conditions.

Shukla *et al.* (2011) simulated the three-dimensional flow of a Francis turbine, followed by a validation of the results with experimental data. The 3D model of the turbine components was performed in the Pro-E software and the numerical simulation in Ansys. The experimental data were obtained by using a turbine model in a wind tunnel. This dataset underwent upscaling after its acquisition. The results indicated that the maximum efficiency regime in both cases was almost equal. However, the flow of the streamlines was more turbulent due to the occurrence of losses. The deviations between the datasets were attributed to instrumental and human errors in the experiment, domain discretisation errors, and the solution of the differential equations.

Choi *et al.* (2013) used CFD to optimise a Francis turbine design. The flow of a Francis turbine was simulated with measurements already specified in the Ansys CFX software; the data obtained were analysed, and a series of modifications were made to the project. The simulation results closely matched the experimental data, with a maximum error of 1.5%. Furthermore, it was observed that the modifications could provide an increase of approximately 9.93% in the maximum efficiency of the turbine.

Teran *et al.* (2016) used a CFD analysis to obtain an alternative geometry for a more efficient 500 kW Francis turbine. The first part of the work focused on the spiral case, the fixed vanes, the guide vanes, and some regions of the impeller. The second part focused on improving the blade profile of the impeller using factorial experiments, artificial neural networks, and optimisation based on genetic algorithms. The results indicated an increase of 14.77% in turbine efficiency at full power and a possible increase in energy production of 16.4% if the appropriate flow rate is provided. In addition, cavitation and axial forces were minimised. A mechanical analysis indicated that the new geometry has good safety factors regarding mechanical strength and the risk of resonance.

Kocak *et al.* (2017) designed a Francis turbine impeller using the Bovet method and made a flow simulation using Ansys BladeGen and Ansys CFX software. It was observed that the turbine efficiency in the simulation deviated by only 1% from that calculated by the Bovet method, proving its reliability for preliminary impeller design and pointing to possible design improvements.

Rousseau *et al.* (2021) simulated a Francis turbine's transient flow and evaluated the efficiency increase caused by rehabilitating the static blades. Ansys CFX software was used to compute the turbulent flow. Experimental data from two turbines that had their static blades rehabilitated was used to validate the model. The numerical results were close to the experimental ones; however, the model is less accurate than the experiments in the efficiency calculations.

The study by Hidalgo *et al.* (2022) developed a methodology to simulate the steady-state flow of a Francis turbine. The OpenFOAM software was employed with the Multiple Reference Frame (MRF), which defines a rotating reference for the impeller and a static reference for the spiral case, mimicking the rotary motion, and the Arbitrary Mesh Interface (AMI), which allows simulation along adjacent and disconnected meshes. Experimental data were taken from one of the turbines at the San Francisco hydroelectric power plant in Ecuador. The results showed that the methodology could successfully reproduce fluid flow in a Francis turbine, where the lowest relative error achieved by the k-ε model was 5.02% in terms of power.

In this work, the design and simulation of the flow in a Francis turbine impeller were carried out in Ansys Student 2023 R2. Performance parameters such as torque, head, efficiency, and shaft power, as well as the characteristic curves of shaft power and efficiency, were obtained to present CFD as an auxiliary tool for the design of hydraulic turbines.

2. METHODOLOGY

2.1 Finite Volume Method

It is a method where the partial differential equation is integrated around control volumes and time when in a transient state, expressed in its conservative form, and then discretised (Versteeg and Malalasekera, 2007; Zikanov, 2010). This numerical method follows the laws of conservation of mass and energy and is widely used in commercial software because of it (Maliska, 2014).

This method can be coupled with unstructured meshes, enabling its application in complex geometries, automatic mesh generation, and high flexibility and control of mesh parameters such as the size and number of cells (Zikanov, 2010).

2.2 Turbulence model k-ε

A characteristic of turbulent flows is the presence of fluctuating velocity fields where high-frequency and small-scale fluctuations make the computational cost of the simulation very high due to the large amount of information needed to describe the flow (Andersson *et al.*, 2012). However, most engineering applications do not require the solution of the fluctuations, so methods based on the Reynolds Average Navier-Stokes Equation (RANS) are used (Versteeg and Malalasekera, 2007). This approach modifies the equations, simplifying them but increasing the number of unknown variables, with the turbulence models determining the new variables and enabling the system of equations solution (Andersson *et al.*, 2012).

The effects of fluctuations are analysed by implementing the Reynolds decomposition in the continuity and Navier-Stokes equations, resulting in Eq. (1) to (4), with the last three being called the RANS equations for incompressible flow (Versteeg and Malalasekera, 2007).

$$\nabla \cdot \boldsymbol{U} = 0 \tag{1}$$

$$\frac{\partial U}{\partial t} + \nabla \cdot (\rho U \boldsymbol{U}) = -\frac{1}{\rho}\frac{\partial p}{\partial x} + \nabla \cdot (\mu \nabla U) + \frac{1}{\rho}\left[\frac{\partial(-\rho\overline{u'^2})}{\partial x} + \frac{\partial(-\rho\overline{u'v'})}{\partial y} + \frac{\partial(-\rho\overline{u'w'})}{\partial z}\right] \tag{2}$$

$$\frac{\partial V}{\partial t} + \nabla \cdot (\rho V \boldsymbol{U}) = -\frac{1}{\rho}\frac{\partial p}{\partial y} + \nabla \cdot (\mu \nabla \mathrm{V}) + \frac{1}{\rho}\left[\frac{\partial(-\rho\overline{u'v'})}{\partial x} + \frac{\partial(-\rho\overline{v'^2})}{\partial y} + \frac{\partial(-\rho\overline{v'w'})}{\partial z}\right] \tag{3}$$

$$\frac{\partial W}{\partial t} + \nabla \cdot (\rho W \boldsymbol{U}) = -\frac{1}{\rho}\frac{\partial p}{\partial z} + \nabla \cdot (\mu \nabla W) + \frac{1}{\rho}\left[\frac{\partial(-\rho\overline{u'w'})}{\partial x} + \frac{\partial(-\rho\overline{v'w'})}{\partial y} + \frac{\partial(-\rho\overline{w'^2})}{\partial z}\right] \tag{4}$$

The k-ε turbulence model employed uses two transport equations to obtain the turbulence properties of the fluid, Eq. (5) for the turbulent kinetic energy (k) and Eq. (6) for the viscous dissipation rate (ε).

$$\frac{\partial(\rho k)}{\partial t} + \nabla \cdot (\rho k U) = \nabla \cdot \left[\left(\frac{\mu_t}{\sigma_k}\nabla k\right)\right] + 2\mu_t S_{ij}.S_{ij} - \rho\varepsilon \tag{5}$$

$$\frac{\partial(\rho \varepsilon)}{\partial t} + \nabla \cdot (\rho \varepsilon U) = \nabla \cdot \left[\left(\frac{\mu_t}{\sigma_\varepsilon}\nabla \varepsilon\right)\right] + C_{1\varepsilon}\frac{\varepsilon}{k}2\mu_t S_{ij}.S_{ij} - C_{2\varepsilon}\rho\frac{\varepsilon^2}{k} \tag{6}$$

where S_{ij} is the average strain rate.

The physical meanings of the terms in Eq. (5) and (6) are analogous; thus, the first term on the left-hand side of both equations is the rate of change of k or ε, the second is the transport of k or ε by convection. The first term on the right-hand side is the transport of k or ε by diffusion, the second is the production rate of k or ε, and the third is the destruction rate of k or ε (Andersson *et al.*, 2012).

The large-scale turbulence effects are defined by Eq. (7) and (8), which represent the velocity scale (ϑ) and the length scale (ℓ), respectively. The turbulence viscosity (μ_t) can be obtained by Eq. (9).

$$\vartheta = k^{\frac{1}{2}} \tag{7}$$

$$\ell = \frac{k^{\frac{3}{2}}}{\varepsilon} \tag{8}$$

$$\mu_t = C\rho\vartheta\ell = \rho C_\mu \frac{k^2}{\varepsilon} \tag{9}$$

Constants C_μ, σ_k, σ_ε, $C_{1\varepsilon}$, and $C_{2\varepsilon}$ were used to close the equations of the k-ε model, simplifying them. The values adopted for each constant are: 0.09, 1.00, 1.30, 1.44, and 1.92, respectively. Although there are small variations from one flow to another, they are considered universal (Andersson *et al.*, 2012).

2.3 Impeller design

The following design method was developed by the Swiss engineer Theodore Bovet in 1963 and is focused on obtaining a set of parameters used in determining the size of the meridional profile of the blade and the impeller channel of a Francis turbine, as shown in Figure 1 (Macyntire, 1983).

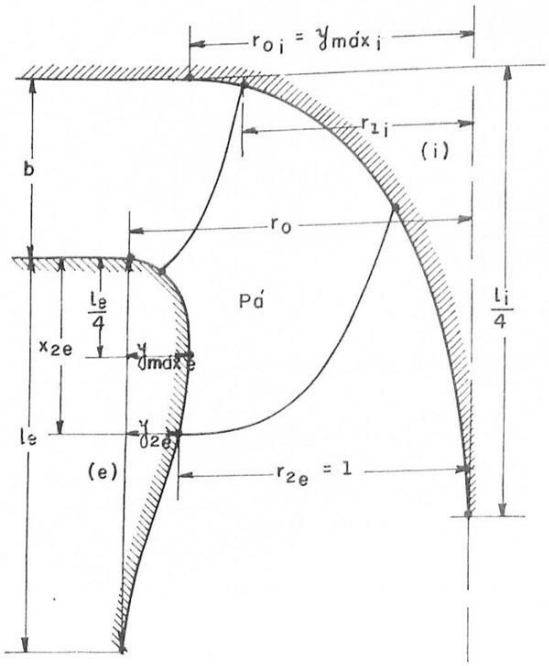

Figure 1. Meridional profile of the impeller's blade and channel shown in Macyntire (1983).

The specific speed (n_s), as described by Eq. (10), is a characteristic parameter of the turbine that associates three basic quantities of the turbine design: head (H), power (N), and the impeller's rotation speed (n).

$$n_s = n\frac{\sqrt{N}}{\sqrt[4]{H^5}} \tag{10}$$

The velocity coefficient (n_0) can be calculated by Eq. (11).

$$n_0 = 1.83x10^{-3}n_s \tag{11}$$

The height of the leading edge (b) can be obtained by employing Eq. (12).

$$b = 0.8(2 - n_0)n_0 \tag{12}$$

The radius of the point where the curvature of the inner meridional line begins (r_{0i}) can be obtained by Eq. (13).

$$r_{0i} = 0{,}7 + \frac{0{,}16}{n_0 + 0{,}08} \tag{13}$$

The height of the inner meridional thread (l_i) can be calculated by Eq. (14).

$$l_i = 3.2 + 3.2(2 - n_0)n_0 \tag{14}$$

The height of the outer meridional thread (l_e) can be obtained by employing Eq. (15).

$$l_e = 2.4 - 1.9(2 - n_0)n_0 \tag{15}$$

The equation used to calculate the radius of the point where the curvature of the outer meridional line begins (r_{0e}) depends on the velocity coefficient.

For $n_0 < 0.275$ Eq. (16) is used.

$$r_{0e} = \frac{0{,}493}{n_0^{\frac{2}{3}}} \tag{16}$$

For $n_0 > 0.275$ Eq. (17) is used.

$$r_{0e} = 1{,}255 - 0{,}3n_0 \tag{17}$$

The meridional curves (y) can be calculated by Eq. (18).

$$y = 3.08 y_{máx}\left(1 - \frac{x}{l}\right)\sqrt{\frac{x}{l}\left(1 - \frac{x}{l}\right)} \tag{18}$$

Equation (19) represents the abscissa of the point on the outer meridional line (x_{2e}) defined by Bovet.

$$x_{2e} = 0.5 \tag{19}$$

The ordinate (y_{2e}) of the point on the outer meridional line can be obtained employing Eq. (20).

$$y_{2e} = r_{0e} - 1 \tag{20}$$

The maximum point of the inner meridional line ($y_{máx,i}$) can be calculated by Eq. (21).

$$y_{máx,i} = r_{0i} \tag{21}$$

The values recommended by Bovet for the outlet section radius (r_{2e}), discharge coefficient (δ), and pressure coefficient (φ) are 1, 0.27, and 1.72, respectively.

The relative radius (r_{1i}) can be calculated by Eq. (22).

$$r_{1i} = \frac{0{,}493}{n_0^{\frac{2}{3}}} \tag{22}$$

The angular velocity (ω) can be calculated by Eq. (23).

$$\omega = \frac{\pi n}{30} \tag{23}$$

Previously, it was assumed that r_{2e} was equal to 1, so to draw the real meridional profile of the blade, the parameters must be multiplied by the maximum exit radius (R_{2e}), calculated by Eq. (24).

$$R_{2e} = \left(\frac{Q}{\pi\omega\delta}\right)^{\frac{1}{3}} \tag{24}$$

The height of the real leading edge (B_{real}) can be obtained by employing Eq. (25).

$$B_{real} = bR_{2e} \tag{25}$$

The radius of the point where the curvature of the real inner meridional line begins (R_{0ireal}) can be calculated by Eq. (26).

$$R_{0ireal} = r_{0i}R_{2e} \tag{26}$$

The upper entrance radius (R_{1i}) can be obtained by employing Eq. (27).

$$R_{1i} = r_{1i}R_{2e} \tag{27}$$

The real inner meridional thread height (l_{ireal}) can be calculated by Eq. (28).

$$l_{ireal} = l_i R_{2e} \tag{28}$$

The real outer meridional thread height (l_{ereal}) can be obtained by employing Eq. (29).

$$l_{ereal} = l_e R_{2e} \tag{29}$$

The radius of the point where the curvature of the real outer meridional line begins (R_{0ereal}) can be calculated by Eq. (30).

$$R_{oereal} = r_{0e}R_{2e} \tag{30}$$

The real abscissa (x_{2ereal}) of the point on the outer meridional line can be obtained by employing Eq. (31).

$$x_{2ereal} = x_{2e}R_{2e} \tag{31}$$

The real ordinate (Y_{2ereal}) of the point on the outer meridional line can be calculated by Eq. (32).

$$Y_{2ereal} = y_{2e}R_{2e} \tag{32}$$

The real maximum point of the inner meridional line ($y_{máx,i,real}$) can be calculated by Eq. (33).

$$y_{máx,i,real} = r_{0i}R_{2e} \tag{33}$$

To calculate the maximum point of the outer meridional line ($y_{máx,e}$), it was necessary to reorganize Eq. (18) and apply the values of x_{2e}, y_{2e}, and l_e, resulting in Eq. (34).

$$y_{máx,e} = \frac{3{,}08}{y_{2e}\left(1-\frac{x_{2e}}{l_e}\right)\sqrt{\left(\frac{x_{2e}}{l_e}\left(1-\frac{x_{2e}}{l_e}\right)\right)}} \tag{34}$$

The maximum point of the real outer meridional line ($y_{máx,e,real}$) can be obtained employing Eq. (35).

$$y_{máx,e,real} = y_{máx,e}R_{2e} \tag{35}$$

The pitch (t) of the rotor's blade can be obtained by employing Eq. (36).

$$t = \frac{\pi d}{Z} \tag{36}$$

where Z is the number of blades and d is the diameter of the impeller's circumference.

In the impeller's inlet, not all the area is used for fluid flow due to the blade's thickness. The shrinkage coefficient (v) associates the flow area to the area of the entire section if the blades had no thickness, ranging from 0.88 for smaller turbines to 0.92 for larger turbines (Macyntire, 1983).

The impeller blade angle (β) can be calculated by Eq. (37).

$$\beta = \sin^{-1}\frac{S}{t(1-v)} \tag{37}$$

where S is the blade's thickness.

The input parameters required for the impeller's design were taken from Macyntire (1983), namely flow rate, head, rotation speed, power, and number of blades of the Francis turbine installed at the Luiz Carlos Barreto de Carvalho (Estreito) power plant. The values of each parameter were 339 m^3/s, 63.3 m, 112.5 rpm, 260,000 cv and 16, respectively.

2.4 CFD Software

The CFD analysis was made with Turbomachinery Fluid Flow and its submodules, BladeGen, Turbo Mesh, CFX-Pre, CFX-Solver, and CFX-Post. BladeGen generated the impeller's 3D geometry based on the meridional profile calculated using Bovet's method. The number of blades, the blade's thickness, and the type of turbomachinery were also set. Nine meshes were created on Turbo Mesh for simulation and mesh convergence analysis. On CFX-Pre, CFX-Solver, and CFX-Post, the boundary conditions and turbulence model were set, the solver configurations were defined, and the results were plotted, respectively.

Figures 2a, 2b and 2c show the boundaries on the impeller's channel. The selected turbomachinery was a radial turbine. Simulations were performed on a single blade, excluding the guide and stay vanes. A mass flow rate boundary of 337,983 kg/s with 5% turbulence intensity was used on the inlet. The flow's radial and axial components had angles of 23,087˚ and 0˚, respectively. No-slip wall boundary conditions were placed on the shroud and hub. On the side walls, rotational periodic boundary conditions were used. A rotational speed of 112.5 rpm was used. An average static pressure boundary condition of 1 atm was placed on the outlet.

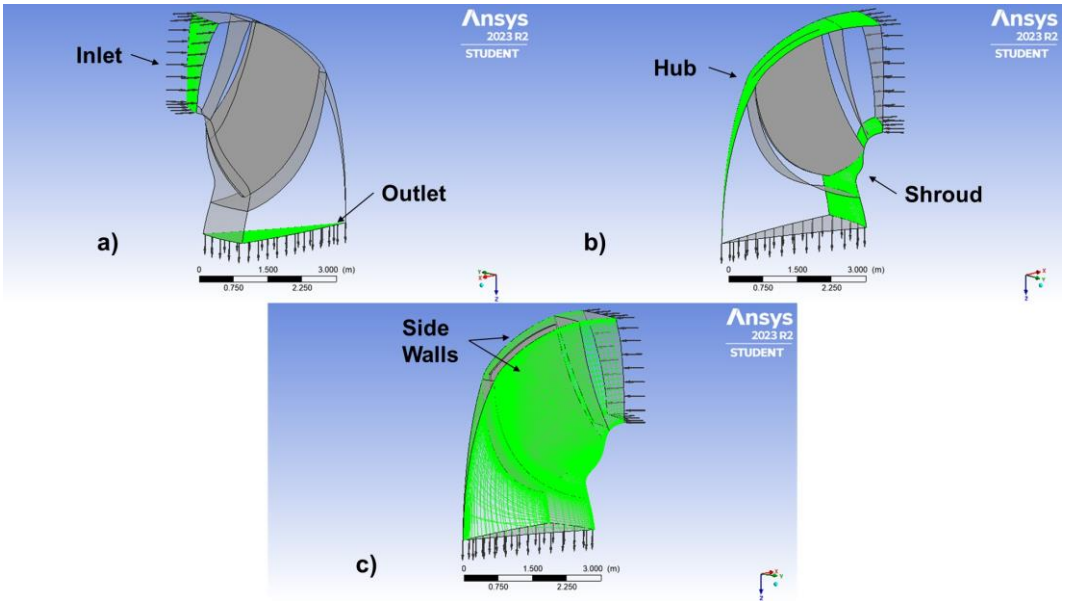

Figure 2. Inlet and outlet a), hub and shroud b) and side wall c) boundaries of the impeller's channel.

The k-ε model and the high resolution advection scheme were employed to simulate the steady-state fluid flow in the impeller. The Rooted Mean Square (RMS) residual error was set to 10^{-5} to ensure the CFD model's accuracy and convergence. The simulation was set to stop at 1,500 iterations if the calculations did not reach the specified RMS value.

3. RESULTS AND DISCUSSION

Figure 3 shows the impeller's efficiency versus the number of nodes in the computational mesh. There were large oscillations in the efficiency value for meshes with nodes smaller than 500,000. The efficiency value started to stabilise for meshes with more than 700,000 nodes. However, mesh convergence could only be verified using meshes with more than 1,000,000 nodes, which wasn't possible because of license restrictions.

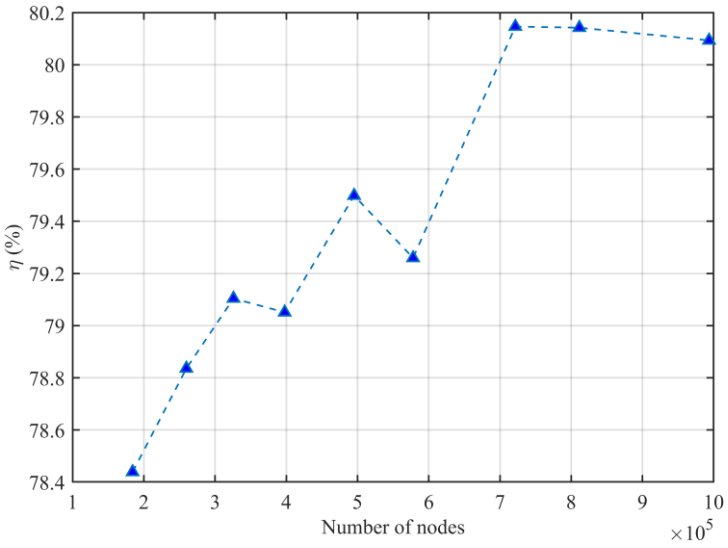

Figure 3. Impeller's efficiency versus number of nodes in the computational mesh.

Figures 4a, 4b, 4c, and 4d show the impeller and the streamlines in the top view, bottom view, and side view, respectively. Fluid flow followed a predominantly radial trajectory, with the velocity increasing from the leading edge to the trailing edge of the blades, a behaviour that agrees with the literature. A portion of the fluid collided with the blades in the inlet region and was projected in the impeller's direction of rotation. Additionally, flow separation at the site reduced impeller efficiency and stimulated vortex formation in the impeller's channels.

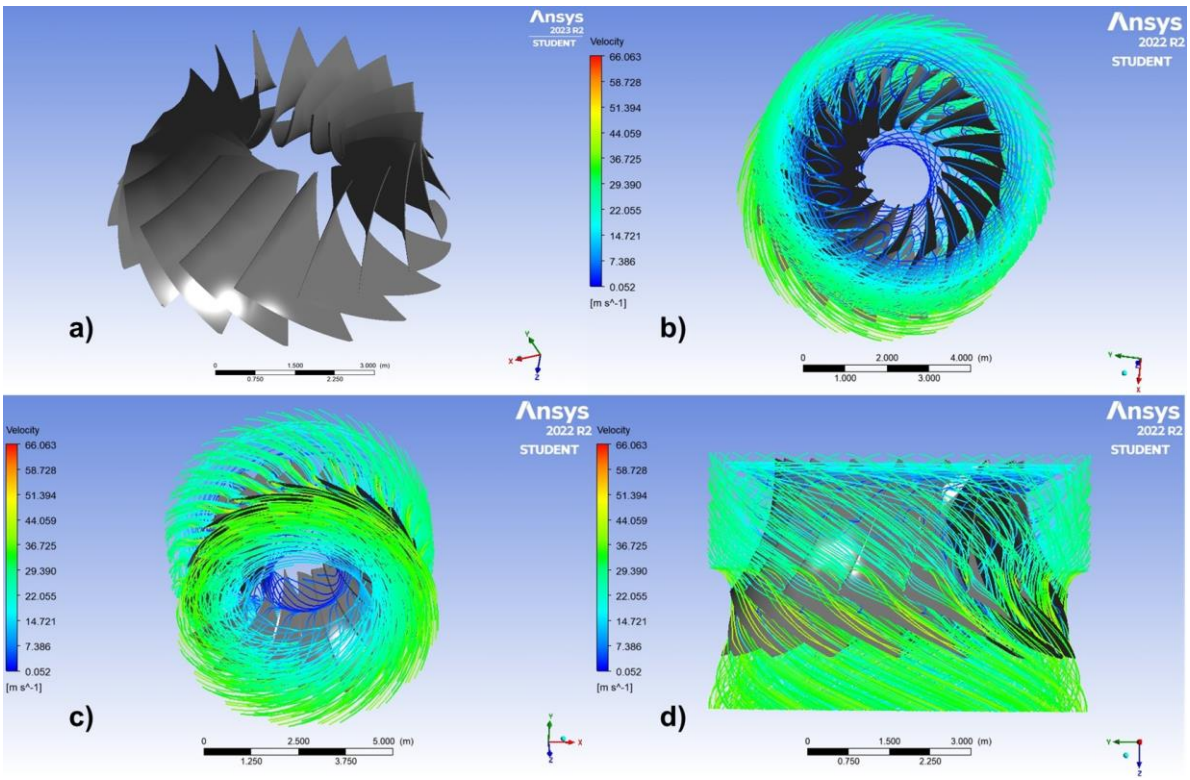

Figure 4. Impeller a) and streamlines in top view b), bottom view c) and side view d).

Figures 5a and 5b show the pressure distribution on the pressure and suction sides of one of the impeller blades, respectively. On both sides, the pressure decreased from the leading edge to the trailing edge, a behaviour that agrees with the literature. Stagnation also occurred at the inlet edge, reducing the fluid flow velocity and increasing the pressure in the region. In addition, the pressure values were larger on the pressure side of the blade than on the suction side, with this pressure difference being responsible for generating torque in the impeller (Choi *et al.*, 2013).

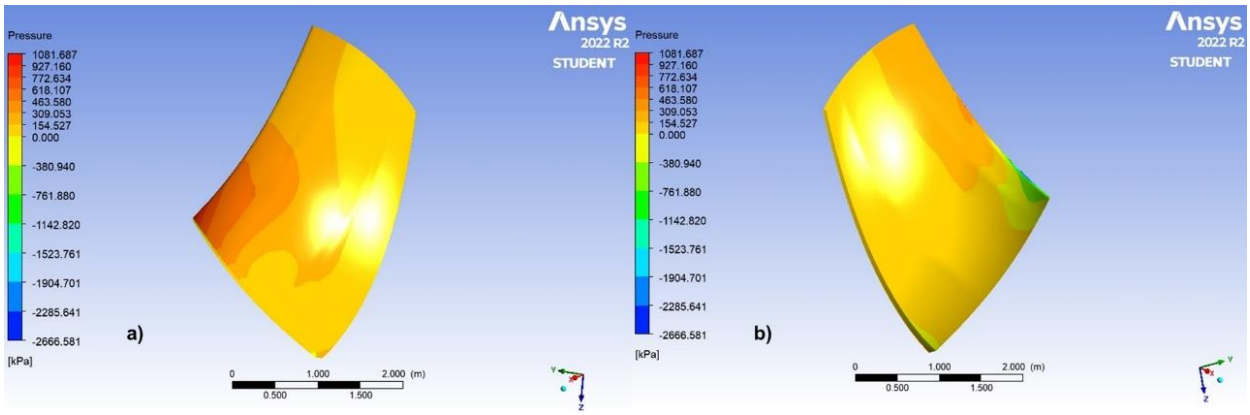

Figure 5. Pressure distribution on the pressure side a) and suction side b).

On the pressure side, the largest pressure values are encountered in the lower region of the leading edge. In this same region, but on the suction side, there was a pressure drop, a phenomenon found in most Francis turbines and usually causes damage due to cavitation at the site (Wu *et al.*, 2007). In addition, a pressure peak on one side of the blade and a pressure drop on the opposite side indicate an impact effect at the site, causing an impact loss in the impeller (Choi *et al.*, 2013).

Table 1 shows the values of the performance parameters provided by the software, the values taken from Macyntire (1983), and the relative error between the two. The parameters obtained through the simulation were close to those found

in the literature, with a maximum relative error of 11%. To reduce the error, it is necessary to use a specific calculation method for the blade streamlines and to apply a variable blade thickness.

Table 1. Relative error between literature data taken from Macyntire (1983) and those calculated.

Data	Head	Power	Efficiency	Torque
Literature value	63.30 m	260,000.00 cv	90.00 %	16,232,000 N.m
Calculated value	64.12 m	231,441.20 cv	80.09 %	14,449,100 N.m
Relative error	1.13 %	10.98 %	11.00 %	10.98 %

The head value provided by the simulation was larger than the one in the literature due to numerical instabilities related to the turbulence model and the less refined computational mesh, which overestimated the difference between the head at the impeller inlet and outlet.

The efficiency provided by the simulation was reduced due to impact loss, flow separation, and vortices between the blades, making it necessary to change the leading edge angle as well as the geometry and angle of the impeller blades to reduce or avoid these types of losses (Choi *et al.*, 2013).

Power and torque showed large errors because they were obtained from other parameters, and error propagation occurred during the calculations.

Figures 6a and 6b show the efficiency and power curves as a function of flow rate, respectively. The efficiency curve slope indicated this parameter growth with increasing flow rates. This behaviour doesn't agree with the literature, as there should be an increase, followed by stabilisation at an optimum value, and then a decrease until the final value (Henn, 2006).

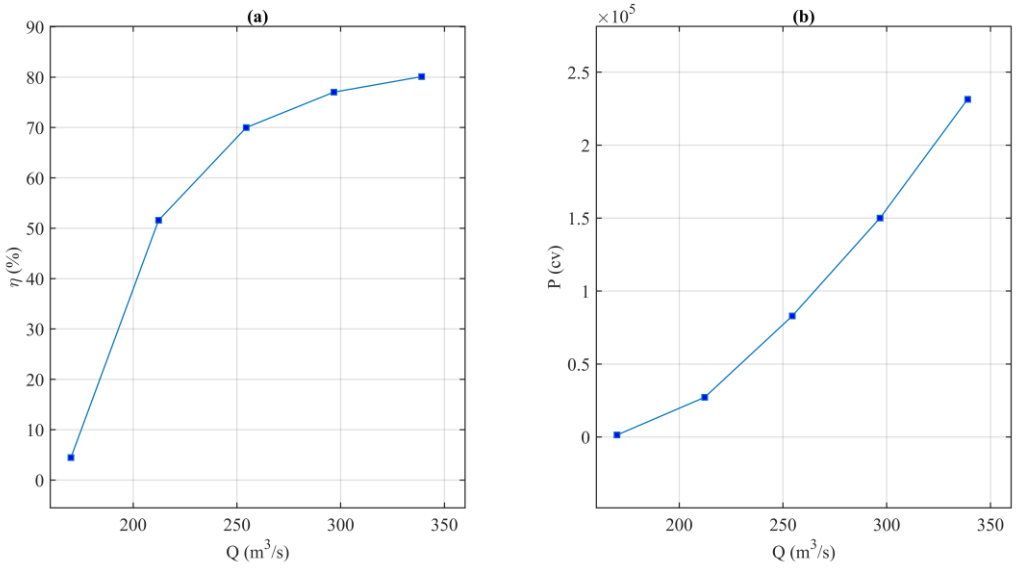

Figure 6. Efficiency curve a) and power curve b).

The inconsistencies in the efficiency curve were related to numerical instabilities arising from the computational mesh and the turbulence model. Improvements in mesh refinement should improve the curve's behaviour. Additionally, comparing different turbulence models could indicate one that can reproduce the efficiency curve more accurately. The slope of the power curve indicated an approximately linear growth of this parameter with increasing flow rates, a behaviour that agrees with the literature (Henn, 2006).

4. CONCLUSION

In this work, a Francis turbine impeller was designed and simulated to present CFD as an auxiliary tool to the design process of hydraulic turbines. The fluid flow, the performance of the designed impeller, and the error between the data obtained and those of the literature were analysed.

Part of the fluid collided with the blades and was projected in the impeller's rotation direction. The impeller's streamline velocity agreed with the literature, being larger at the trailing edge than at the leading edge.

The pressure distribution on both sides of the impeller blade mostly agreed with the literature, larger on the leading edge than on the trailing edge. Further, the pressure drop on the suction side of the blade can cause cavitation damage at the site, a recurring problem in Francis turbines.

The losses caused by the impact effect, flow separation, and formation of vortices between the impeller blades reduced the device's efficiency. The relative errors between the performance parameters obtained and the literature data were about 11%, showing the proximity between the two.

Unlike the power curve, the efficiency curve behaviour did not agree with the literature, with such inconsistency being related to numerical instabilities arising from the computational mesh and the turbulence model. Using a more refined mesh should minimise the inconsistencies. Moreover, different turbulence models should be evaluated to indicate a more accurate alternative.

For future work, an optimisation method such as genetic algorithms could be used to find the optimum blade profile for a hydraulic turbine's impeller to evaluate the performance improvements over the original design.

5. ACKNOWLEDGMENTS

To the Federal University of Maranhão (UFMA) for providing the necessary structure to carry out this work.

6. REFERENCES

ANEEL, 2022. *ANEEL's Generation Information System (SIGA) (in Portuguese)*. https://app.powerbi.com/view?r=eyJrIjoiNjc4OGYyYjQtYWM2ZC00YjllLWJlYmEtYzdkNTQ1MTc1NjM2Iiwid CI6IjQwZDZmOWI4LWVjYTctNDZhMi05MmQ0LWVhNGU5YzAxNzBlMSIsImMiOjR9. Accessed 28 Set 2022.

Andersson, B., Andersson, R., Hakansson, L., Mortensen, M., Sudiyo, R., and van Wachem, B., 2012. *Computational Fluid Dynamics for Engineers*. Cambridge University Press, New York.

British Petroleum Company, 2022. *Statistical Review of World Energy*. British Petroleum Company, London. https://www.bp.com/content/dam/bp/business-sites/en/global/corporate/pdfs/energy-economics/statistical review/bp-stats-review-2022-full-report.pdf. Accessed 12 May 2022.

Choi, H. J., Zullah, M. A., Roh, H.-W., Ha, P.-S., Oh, S.-Y., and Lee, Y.-H., 2013. CFD validation of performance improvement of a 500 kW Francis turbine. Renewable Energy. Vol. 54, pp. 111-123.

EPE, 2022. *National Energy Balance 2022, Final Report (in Portuguese)*. Empresa de Pesquisa Energética EPE, Rio de Janeiro. https://www.epe.gov.br/sites-pt/publicacoes-dados-abertos/publicacoes/PublicacoesArquivos/publicacao 675/topico-638/BEN2022.pdf. Accessed 12 May 2022.

Henn, E. A. L., 2006. *Fluid Machines (in Portuguese)*. 2 ed. Editora da Universidade Federal de Santa Maria, Porto Alegre.

Hidalgo, V., Velasco, M., Cando, E., Valencia, E., Simbaña, S., Puga, D., Mora, C., and Escaler, X., 2022. Rotatory 3d structured mesh study using openFOAM to simulate the flow in francis turbine. Materials Today: Proceedings, Vol. 49, pp. 142-148.

Kocak, E., Karaaslan S., Yucel, N., and Arundas, F., 2017. A numerical case study: Bovet approach to design a Francis turbine runner. Energy Procedia, Vol. 111, p. 885-894.

Macyntire, A. J., 1983. *Hydraulic Drive Machines (in Portuguese)*. Guanabara Dois, Rio de Janeiro.

Maliska, C. R., 2014. *Heat transfer and computational fluid mechanics (in Portuguese)*. 2 ed. LTC, Rio de Janeiro.

Rousseau, P. M., Soulaimani, A., and Sabourin, M., 2021. Efficiency Assesment for Rehabilitated Francis Turbine Using URANS Simulations. Water, Vol. 13, pp. 1-23.

Shukla, M. K., Prasad, V., Rajeev, J., and Shukla, S. N., 2011. CFD Analysis of 3-D Flow for Francis Turbine. MIT International Journal of Mechanical Engineering. Vol. 1, pp. 93-100.

Teran, L. A., Larrahondo, F. J., and Rodríguez, S. A., 2016. Performance Improvement of a 500-kW Francis turbine based on CFD. Renewable Energy. Vol. 96, pp. 977-992.

Versteeg, H. K and Malalasekera, W., 2007. *An Introduction to Computational Fluid Dynamics: The Finite Volume Method*. 2 ed. Pearson Education Limited, Edinburgh Gate.

Wu, J., Shimmei, K., Tani, K., Niikura, K., and Sato, J., 2007. CFD-Based Design Optimization for Hydro-Turbines. Journal of Fluids Engineering, Vol. 129, pp. 159-168.

Zikanov, O., 2010. *Essential Computational Fluid Dynamics*. John Wiley & Sons, Inc, Hoboken.

7. RESPONSIBILITY NOTICE

The authors are the only ones responsible for the printed material included in this paper.